Available online at www.sciencedirect.com
ScienceDirect
Journal of Constructional Steel Research 63 (2007) 779–790
JOURNAL OF CONSTRUCTIONAL STEEL RESEARCH
www.elsevier.com/locate/jcsr

# Model of local buckling in steel hollow structural elements subjected to biaxial bending

Néstor Guerrero[a,b], María Eugenia Marante[b,*], Ricardo Picón[b], Julio Flórez-López[a]

[a] Department of Structural Engineering, University of Los Andes, Mérida 5101, Venezuela
[b] Department of Structural Engineering, Lisandro Alvarado University, Barquisimeto, Venezuela

Received 30 March 2006; accepted 14 August 2006

**Abstract**

This paper presents a general formulation for the analysis of steel hollow structural beams subjected to biaxial bending. The model has been developed within the framework of lumped damage mechanics. In this approach, the models are based on methods of continuum damage mechanics and the concept of plastic hinge. The model was implemented in a commercial finite element program. In order to calibrate the model, a set of experimental tests were carried out in the Structural Mechanics Laboratory at the Lisandro Alvarado University. The model was evaluated by the numerical simulation of these tests finding a good agreement between the experimental tests and the numerical simulations.


*Keywords:* Local buckling; Steel hollow beam sections; Frames; Lumped damage mechanics; Structural analysis; Biaxial bending

## 1. Introduction

Steel tubular structures are more and more frequently used in the construction industry. In most cases, these structures are designed using plasticity theories. However, due to their small wall thickness they are prone to local buckling failure. Davies [1] states that, often, local buckling does not permit the development of a stable strain hardening moment-rotation relationship. Qin et al. [2] found, after an experimental study, that local buckling is the main energy dissipating mechanism in the case of overlap tubular joints of offshore structures subjected to earthquake loading. An already classic example of local buckling failure was the damage observed in a crane of the port of Kobe that occurred during the 1995 earthquake as reported in [3]. The necessity for a better comprehension of this phenomenon and of new and more effective analytical models is clear. Local buckling effects should be included into the routine analysis of tubular structures in seismic areas.

Extensive experimental studies on local buckling have been carried out, many of them on structural elements subjected to axial forces [2,4–9]. Tests on local buckling due to bending effects are less frequently reported in the literature. Lee et al. [10], and Lee and Choi [11] carried out tests on square tube beams under three point bending loads. Echalakani et al. [12] performed cyclic bending tests on compact circular hollow beams. Inglessis et al. [13] and Febres et al. [14] tested cantilever beams of circular hollow sections subjected to cyclic bending loadings. Tests on small-scale [15] and full-scale frames [16,17] have also been reported in the literature. In both cases severe degrees of local buckling appeared in the columns.

The analytical procedures for the analysis of local buckling can be classified into four categories: the use of nonlinear shell theories and the finite element method (see for instance [18–23]), beam theories such as the one proposed in the classic paper by Sohal & Chen [24], semi-empirical methods and lumped damage mechanics [13–15]. The present work can be included in the last category. In lumped damage mechanics, local buckling is concentrated at the plastic hinges. A new internal variable denoted damage is introduced; this variable can take values between zero (plastic hinge without local buckling) and one (total damage). A procedure for the experimental measure of the damage variable was proposed in [13]. The new variables are introduced into the stiffness or flexibility matrices of each frame member and into the yield functions of the plastic hinges. Additional

* Corresponding author. Tel.: +58 251 259 2173; fax: +58 274 240 2867.
*E-mail addresses:* emarante@ucla.edu.ve, marante@ula.ve (M.E. Marante).

0143-974X/$ - see front matter © 2006 Elsevier Ltd. All rights reserved.
doi:10.1016/j.jcsr.2006.08.006

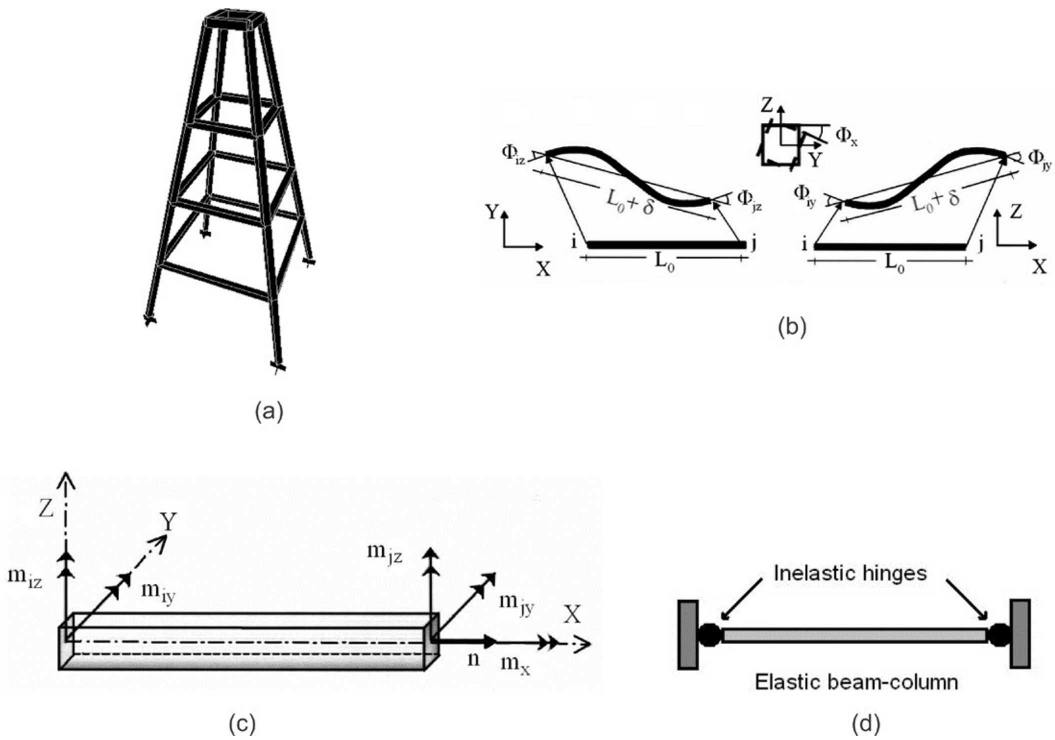


Fig. 1. (a) Framed structure. (b) Generalized stresses of a frame member. (c) Generalized deformations of a frame member. (d) Lumped plasticity model.

evolution laws are included in order to account for local buckling development. The resulting model offers a good compromise between efficacy and accuracy. It is important to note that in large structures, where local buckling appears simultaneously at several locations, significant stiffness and strength redistributions occur. Thus, it is necessary to perform the analysis of the entire structure in order to account for the coupling effects between the different damaged locations. In these cases, lumped damage mechanics is usually the only alternative.

All the aforementioned works on lumped damage mechanics considered only the case of uniaxial bending. In this paper, the lumped damage approach is used to describe local buckling under biaxial conditions. The phenomenon in this case is characterized by the presence of at least two "wrinkles" in different sides of the cross section. The scalar damage parameters proposed in the previous references are substituted by vector variables. The resulting model is however as simple as the previous ones but much more general. Lumped damage mechanics has also been used in the case of reinforced concrete structures [25,26].

This paper is organized as follows. In Section 2, the damage vector variables are introduced and the resulting stiffness and flexibility matrices are derived. The yield function of a three dimensional plastic hinge with biaxial local buckling is presented in Section 3. Local buckling evolution laws are proposed in Section 4 and are based on a new concept: the local buckling domain. This domain can be experimentally obtained and a procedure for its determination is proposed in Section 5. The procedure is applied to the case of square hollow cross sections. Finally, a set of tests on cantilever beams subjected to complex biaxial loading paths are described in Section 6. These tests were used to validate the model and evaluate its limitations.

## 2. Flexibility and stiffness matrices of a steel frame member with local buckling

Consider a steel frame as shown in Fig. 1(a). The generalized stress and deformation matrices of a frame member are: $\{M\}_b^t = (m_{iy}, m_{jy}, n, m_{iz}, m_{jz}, m_x)$ and $\{\Phi\}_b^t = (\phi_{iy}, \phi_{jy}, \delta, \phi_{iz}, \phi_{jz}, \phi_x)$. The mechanical interpretation of the components in those matrices is presented in Fig. 1(b) and (c). The conventional lumped plasticity model will be used for the description of member behavior. Thus, a frame element is assumed to be the assemblage of an elastic beam–column and two plastic hinges as shown in Fig. 1(d). Plastic rotations and deformations are included in the generalized plastic deformation matrix: $\{\Phi_p^t\} = (\phi_{iy}^p, \phi_{jy}^p, \delta^p, \phi_{iz}^p, \phi_{jz}^p, \phi_x^p)$. In order to describe local buckling effects, the lumped damage mechanics approach will be used. Thus, local buckling is assumed to be lumped at the plastic hinges. Under biaxial bending, local buckling in a plastic hinge will be described by a vector variable that will be denoted damage. For a hinge $i$, the damage vector is: $\{\vec{d_i}\} = (0, d_{iy}, d_{iz})$. The components of the damage vector can take values between zero and one, where zero represents the absence of local buckling. A mechanical interpretation of the damage parameters in the case of a beam of hollow rectangular cross section is shown in Fig. 2. It can be noticed that, in this paper, local buckling due to torsional effects is being neglected.

The elasticity law of a frame member with local buckling is the one obtained from lumped damage mechanics (see for

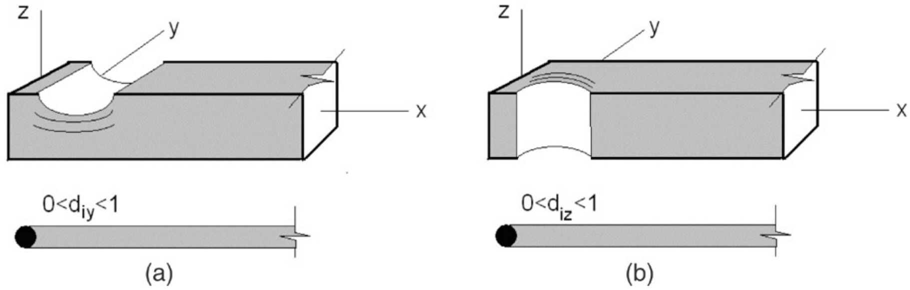


Fig. 2. Characterization of local buckling through damage parameters.

$$[S(\vec{d}_i,\vec{d}_j)] = [F(\vec{d}_i,\vec{d}_j)]^{-1} = \begin{bmatrix} \frac{3S^0_{11}(1-d_{iy})}{4-(1-d_{iy})(1-d_{jy})} & \frac{3S^0_{12}(1-d_{iy})(1-d_{jy})}{4-(1-d_{iy})(1-d_{jy})} & 0 & 0 & 0 & 0 \\ \frac{3S^0_{21}(1-d_{iy})(1-d_{jy})}{4-(1-d_{iy})(1-d_{jy})} & \frac{3S^0_{22}(1-d_{jy})}{4-(1-d_{iy})(1-d_{jy})} & 0 & 0 & 0 & 0 \\ 0 & 0 & S^0_{33} & 0 & 0 & 0 \\ 0 & 0 & 0 & \frac{3S^0_{44}(1-d_{iz})}{4-(1-d_{iz})(1-d_{jz})} & \frac{3S^0_{45}(1-d_{iz})(1-d_{jz})}{4-(1-d_{iz})(1-d_{jz})} & 0 \\ 0 & 0 & 0 & \frac{3S^0_{54}(1-d_{iz})(1-d_{jz})}{4-(1-d_{iz})(1-d_{jz})} & \frac{3S^0_{55}(1-d_{jz})}{4-(1-d_{iz})(1-d_{jz})} & 0 \\ 0 & 0 & 0 & 0 & 0 & S^0_{66} \end{bmatrix}$$

Box I.

instance [25,26]):

$$\{\Phi - \Phi_p\} = [F(\vec{d}_i,\vec{d}_j)]\,\{M\} \tag{1}$$

where $[F(\vec{d}_i,\vec{d}_j)] = [F^0] + [C(\vec{d}_i,\vec{d}_j)]$.

$[F^0]$ is the conventional flexibility matrix as defined in textbooks of structural analysis and $[C(\vec{d}_i,\vec{d}_j)]$ is an additional flexibility term due to local buckling. The expression of this matrix is:

$$[C(\vec{d}_i,\vec{d}_j)] = \begin{bmatrix} \frac{d_{iy}F^0_{11}}{(1-d_{iy})} & 0 & 0 & 0 & 0 & 0 \\ 0 & \frac{d_{jy}F^0_{22}}{(1-d_{jy})} & 0 & 0 & 0 & 0 \\ 0 & 0 & 0 & 0 & 0 & 0 \\ 0 & 0 & 0 & \frac{d_{iz}F^0_{44}}{(1-d_{iz})} & 0 & 0 \\ 0 & 0 & 0 & 0 & \frac{d_{jz}F^0_{55}}{(1-d_{jz})} & 0 \\ 0 & 0 & 0 & 0 & 0 & 0 \end{bmatrix}. \tag{2}$$

The stiffness matrix of a frame member with local buckling is then given in Box I: where $S^0_{ii}$ are the components of the elastic stiffness matrix.

It can be noticed that if the damage variable takes the value zero, there is no additional flexibility. If a damage variable takes the other limit value, the stiffness matrix becomes that of a frame member with an internal hinge. The damage variable is assumed to evolve continuously from zero to one after some evolution law that will be defined in Section 4. In this way, stiffness degradation due to local buckling is represented.

## 3. Yield function of a plastic hinge with local buckling

The plastic behavior of a plastic hinge is defined through a yield function. In the case of a perfectly plastic hinge without local buckling, a conventional expression is given by [27]:

$$f_i = \left(\frac{n}{N_u}\right)^{e_1} + \left(\frac{m_{iy}}{M_{uy}}\right)^{e_2} + \left(\frac{m_{iz}}{M_{uz}}\right)^{e_3} - 1 \tag{3}$$

where $N_u$ is the axial yield load, whereas $M_{uy}$ and $M_{uz}$ are the plastic moments of the section. The constants $e_1$, $e_2$ and $e_3$ are member dependent parameters. In lumped damage mechanics, the yield function of a plastic hinge with damage is obtained by the equivalent stress hypothesis [25,26]. This premise states that the yield function of a damaged plastic hinge can be obtained by the substitution, in the conventional expression, of the moments by the effective ones. The concept of effective moment is similar to the effective stress idea introduced in continuum damage mechanics and poroelasticity and is given by:

$$\bar{m}_{iy} = \frac{m_{iy}}{1-d_{iy}}; \qquad \bar{m}_{iz} = \frac{m_{iz}}{1-d_{iz}}. \tag{4}$$

Therefore, the yield function of a plastic hinge with local buckling is:

$$f_i = \left(\frac{n}{N_u}\right)^{e_1} + \left(\frac{m_{iy}}{M_{uy}(1-d_{iy})}\right)^{e_2} + \left(\frac{m_{iz}}{M_{uz}(1-d_{iz})}\right)^{e_3} - 1. \tag{5}$$

It can be seen that damage decreases the value of the effective plastic moments. Strength degradation due to local buckling is described in this way. Plastic deformation evolution law is now obtained via the normality law:

$$\dot{\phi}^p_{iy} = \dot{\lambda}_i \frac{\partial f_i}{\partial m_{iy}}; \qquad \dot{\phi}^p_{iz} = \dot{\lambda}_i \frac{\partial f_i}{\partial m_{iz}};$$

$$\dot{\delta}^p = \dot{\lambda}_i \frac{\partial f_i}{\partial n} + \dot{\lambda}_j \frac{\partial f_j}{\partial n} \tag{6}$$

where $\lambda_i$ and $\lambda_j$ are the plastic multipliers for, respectively, plastic hinge $i$ and $j$. Plastic multipliers are computed by the consistency condition as usual:

$$\begin{cases} \dot{\lambda}_i = 0 & \text{if } f_i = 0 \text{ and } \dot{f}_i = 0 \\ \dot{\lambda}_i > 0 & \text{if } f_i < 0 \text{ or } \dot{f}_i < 0 \end{cases}. \tag{7}$$

## 4. Local buckling evolution law

In this paper, the introduction of a second inelastic function is proposed : the damage function of a plastic hinge $g_i$ that defines a local buckling domain. Inglessis et al. [15] proposed the use of the cumulated plastic rotation as a local buckling driving force in the case of beams subjected to uniaxial bending. In the present case, that idea is generalized in the following way. It is assumed that the new damage function depends on the variables $P_{iy}$ and $P_{iz}$ that are defined as:

$$\dot{P}_{iy} = |\dot{\Phi}^p_{iy}|; \qquad \dot{P}_{iz} = |\dot{\Phi}^p_{iz}|. \tag{8}$$

The general form of the damage function is given by:

$$g_i = g_i(P_{iy}, P_{iz}; \vec{d}_i) \le 0 \tag{9}$$

where the damage variable is included in (9) in order to describe "hardening" of the local buckling domain. The local buckling evolution laws are then given by the normality rule, therefore:

$$\dot{d}_{iy} = \dot{\gamma}_i \frac{\partial g_i}{\partial P_{iy}}; \qquad \dot{d}_{iz} = \dot{\gamma}_i \frac{\partial g_i}{\partial P_{iy}} \tag{10}$$

where $\gamma_i$ and $\gamma_j$ are denoted damage multipliers and are computed again by the consistency condition:

$$\begin{cases} \dot{\gamma}_i = 0 & \text{if } g_i = 0 \text{ and } \dot{g}_i = 0 \\ \dot{\gamma}_i > 0 & \text{if } g_i < 0 \text{ or } \dot{g}_i < 0 \end{cases}. \tag{11}$$

The damage function depends on the shape of the cross section. A general procedure for the determination of the damage function and the associated damage domain is proposed in Section 5.

## 5. Local buckling domain in the case of hollow steel beams

An experimental program was carried out at the Structural Mechanics Laboratory of the Lisandro Alvarado University [28]. The specimens consisted of steel hollow structural elements with 120 mm square cross section, 4 mm thickness and a free length of 1.28 m. They were built as a cantilever into a heavily reinforced foundation (see Fig. 3). Two servocontrolled 50 ton-capacity hydraulic actuators applied the desired transverse displacement histories. Each actuator was mounted on the frame and connected to the specimens through a steel device, as can be seen in Fig. 3. When the column top is biaxially displaced, the principal axes of the specimen cross section do not coincide any more with the axes of the actuators. Therefore, a numerical procedure had to be developed at the control signal generation level of the transverse displacement history. The same geometric effect was accounted for at the data-treatment level.

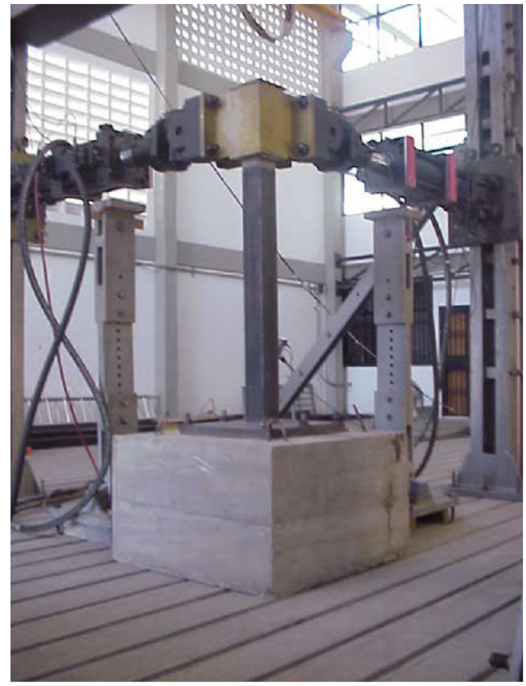

Fig. 3. Setup of a test on cantilever beam.

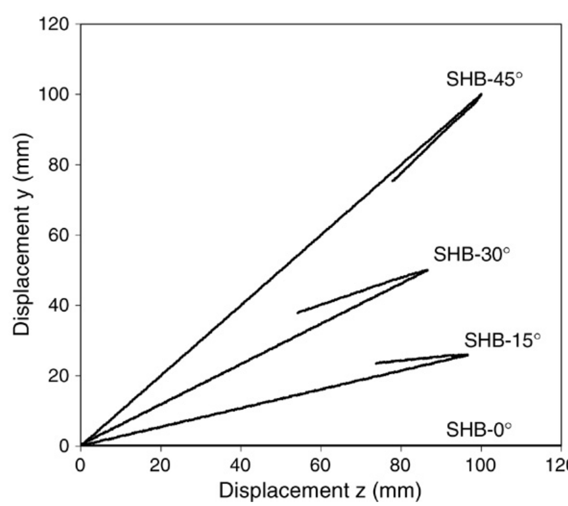


Fig. 4. Loading path in the displacement space.

For the determination of the local buckling domain, four specimens were tested under displacement-controlled conditions, with the loading described in Fig. 4. $t_y$ and $t_z$ are the orthogonal displacements at the top of the beam. It can be noticed that the loading paths in the displacement space are represented by straight lines with different angles with respect to the axis of the $Y$ displacement. These tests will be denoted as SHB-0° (square-hollow-beam at zero degrees), SHB-15°, SHB-30° and SHB-45°.

The experimental results are shown in the graphs of force vs. displacement in the $Z$ and $Y$ directions that are shown in Figs. 5 and 6.

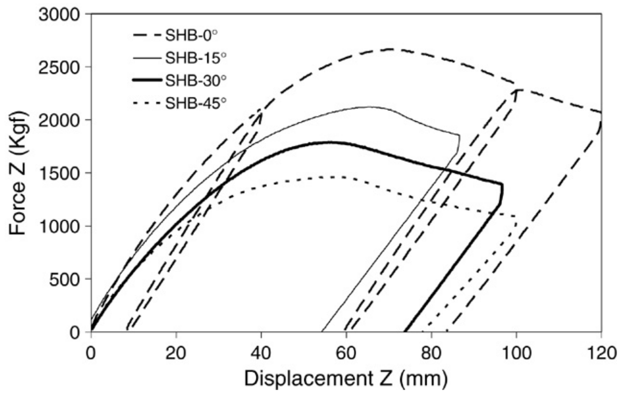


Fig. 5. Force vs. displacement in the $Z$ direction in the SHB-0°, SHB-15°, SHB-30°and SHB-45° tests.

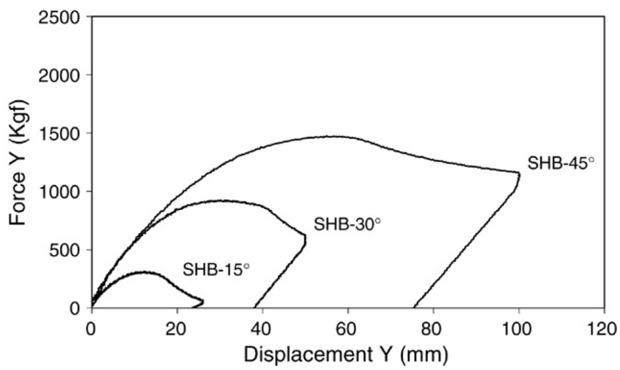


Fig. 6. Force vs. displacement in the $Y$ direction in the SHB-15°, SHB-30°and SHB-45° tests.

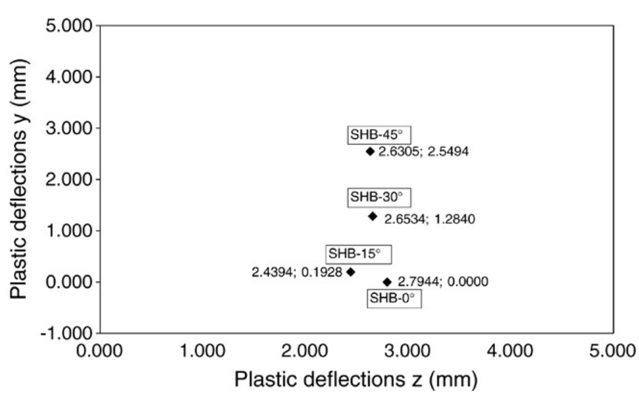


Fig. 7. Experimental determination of the local buckling domain.

Local buckling is assumed to start at the beginning of the softening stage of the test. The plastic deflection at this point is determined by using the slope measured during the elastic stage of the test as shown in Figs. 5 and 6. i.e. it is assumed that the stiffness of the beam remains constant during the hardening stage of the test. The points that correspond to the local buckling start are represented in the space of plastic deflections as shown in Fig. 7.

Thus, in the case of square cross sections, the local buckling domain can be represented as a rectangle as indicated in Fig. 8(a). The local buckling domain increases with damage evolution. It is assumed that during this process, the domain retains the same general form (i.e. only the size of the sides of the rectangle can change). In order to characterize this process, the simplest "hardening term" is adopted. That is, linear functions of the damage parameters are used (see Fig. 8(a)). The constant $P_{cr}$ corresponds to the value of the plastic rotation that initiates local buckling. The constant $c$ measures the growing rate of the local buckling domain. Both constants can be measured in a uniaxial monotonic test (see Fig. 9).

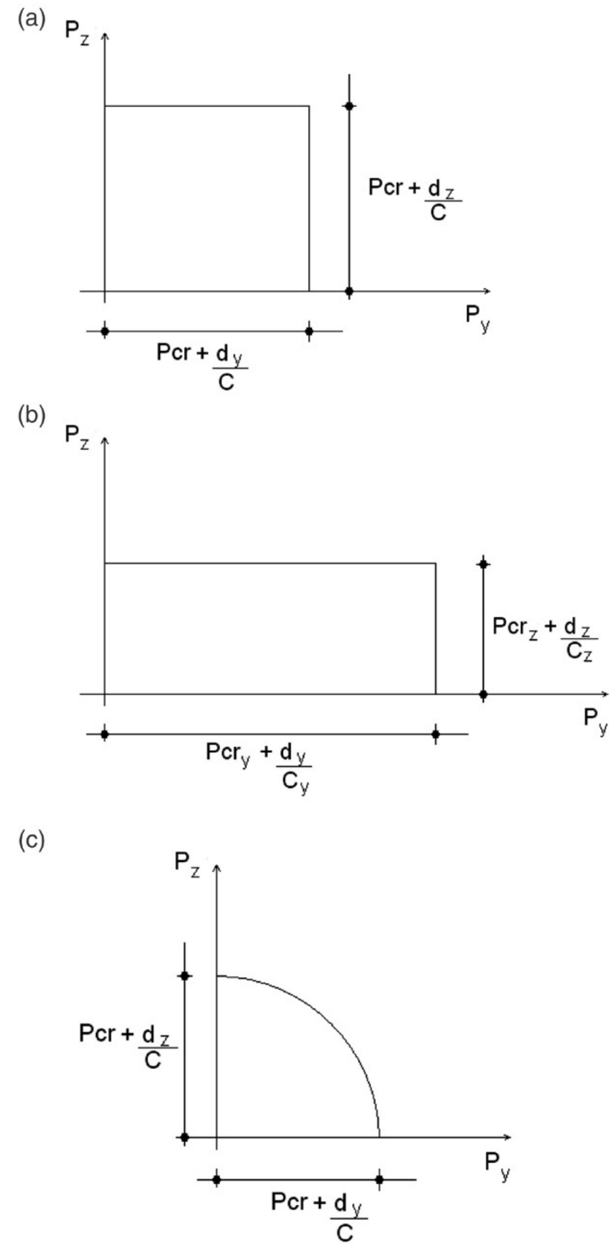


Fig. 8. Local buckling domain. (a) Square hollow cross section. (b) Rectangular hollow cross section. (c) Circular hollow cross section.

The damage evolution law (10) and (11) with the local buckling domain indicated in Fig. 8(a) becomes:

$$d_{iy} = c\left\langle P_{iy} - P_{cr}\right\rangle; \qquad d_{iz} = c\left\langle P_{iz} - P_{cr}\right\rangle. \tag{12}$$

In the case of hollow rectangular elements, the local buckling domain can also be represented by a rectangle as shown in

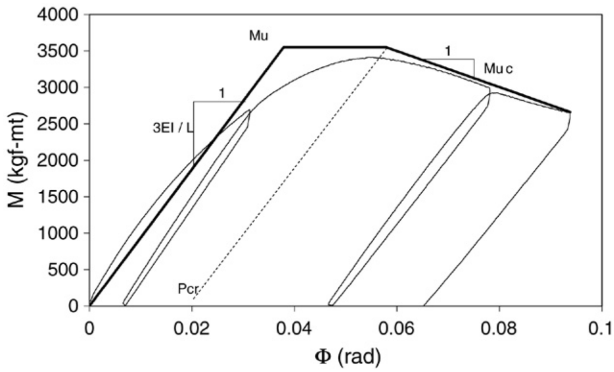


Fig. 9. Experimental determination of the damage evolution law parameters.

Fig. 8(b) [28]. Thus, the damage evolution law becomes:

$$d_{iy} = c_y \left\langle P_{iy} - P_{cry} \right\rangle; \qquad d_{iz} = c_z \left\langle P_{iz} - P_{crz} \right\rangle \tag{13}$$

where $c_y$, $c_z$, $P_{cry}$ and $P_{crz}$ are constants that can also be measured in monotonic uniaxial tests.

In the case of a hollow circular cross section the local buckling domain can be represented by a circle that becomes an ellipse during the "hardening" process (see Fig. 8(c)). The damage function in this case is given by:

$$g_i = \left( \frac{P_{iy}}{P_{cr} + d_{iy}/c} \right)^2 + \left( \frac{P_{iz}}{P_{cr} + d_{iz}/c} \right)^2 - 1. \tag{14}$$

## 6. Experimental analysis and numerical simulations

The model proposed in this paper is therefore composed by the elasticity law (1), the yield function (5), the plastic deformation evolution law (6) and (7), the damage evolution law (10) and (11) and one of the damage functions presented in Section 5. This model was implemented as a new finite element in a commercial structural analysis program [29].

In order to calibrate the model, additional experimental tests were carried out [28]. The specimens were similar to those tested for the local bucking domain determination but they were subjected to much more complex loading paths.

The results of some of these tests are shown in the present section.

### 6.1. Test and simulation SHB-M

In the first test, denoted SHB-M, the specimen is loaded in only one direction with the displacement history shown in Fig. 10(a). The results of this test will be used for the identification of the model parameters. The monotonic behavior predicted by the model can be observed in the simulation of the test. It can be noticed that, in order to observe stiffness degradation due to local buckling, a set of elastic unloadings were also carried out. The experimental results and the corresponding numerical simulation are shown in Fig. 10(b) and (c). The values of damage computed at the beginning of some elastic unloadings are indicated in the latter figure.

It can be seen that the description of the plastic hardening process has been neglected in the model. This was omitted in order to emphasize the local buckling aspect. However, the hardening effect can be included in the model without any difficulty [15]; and it does not modify the expressions of the local buckling domain or evolution law. As mentioned before, the model describes stiffness and strength degradation due to local buckling.

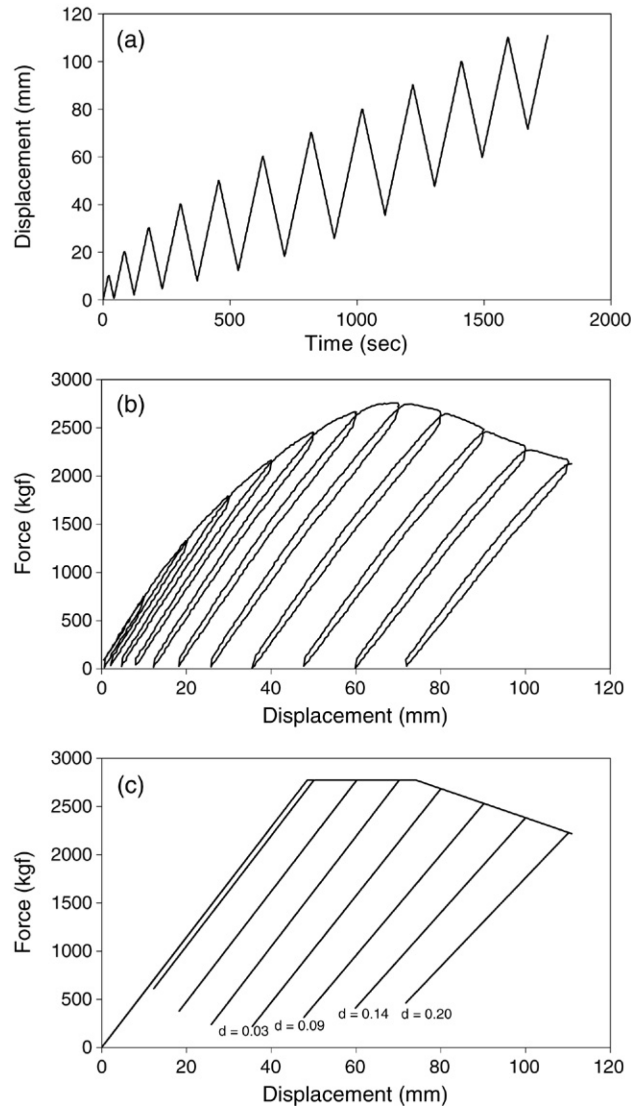


Fig. 10. (a) Loading path of test SHB-M. (b) Experimental force vs. displacement curve. (c) Numerical simulation.

### 6.2. Test and simulation SHB-L

In this test, uniaxial displacements in pairs of linearly increasing amplitude were alternately applied in the two transverse directions. In the space of displacements, the loading is represented by a set of L shaped paths moving away from the origin (see Fig. 11(a)). In Fig. 11(b) is shown the experimental force $Z$–force $Y$ curve and in Fig. 11(c) the curve obtained with the numerical simulation. Fig. 11(d) and (f) show the experimental results in the force–displacement curves and in Fig. 11(f) and (g) the corresponding numerical simulations. A photo of the plastic hinge region at the end of the test is

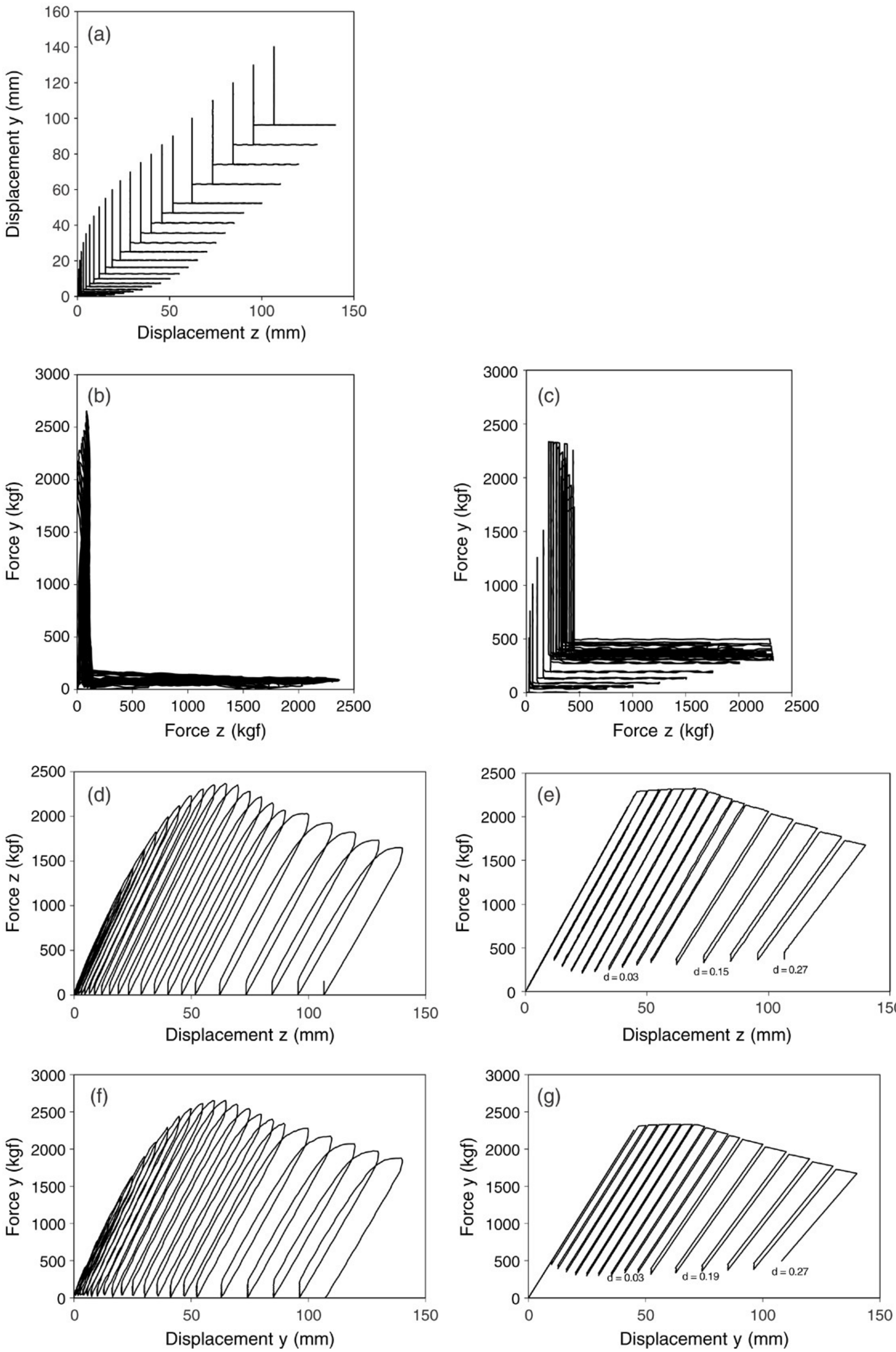


Fig. 11. Test and simulation SHB-L. (a) Imposed transverse displacement path. (b) Experimental force $Z$–force $Y$ curve. (c) Numerical simulation. (d) Experimental force–displacement curve in $Z$ direction. (e) Numerical simulation. (f) Experimental force–displacement curve in $Y$ direction. (g) Numerical simulation.

shown in Fig. 12(b). It can be seen that the local buckling is characterized by the presence of the two wrinkles in two orthogonal sides. This picture can be compared with the local buckling aspect in the case of an uniaxial bending test shown in Fig. 12(a). The values of damage corresponding to different stages of the test are shown in Fig. 11(f) and (g). Thus the

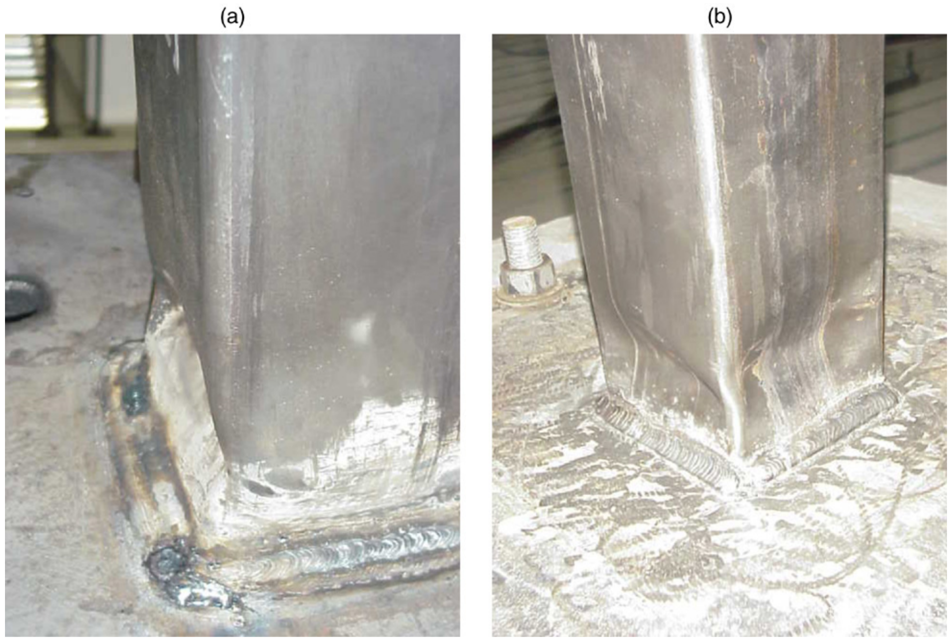

Fig. 12. Local buckling aspect. (a) After an uniaxial bending test. (b) After a biaxial test.

local buckling state in Fig. 12(b) is characterized by the values $d_y = 0.27$ and $d_z = 0.27$.

As mentioned before, all the model parameters were identified with the SHB-M test and they were not modified for the numerical simulation of this test. It can be noticed the good agreement between simulation and experimental results taking into account the simplicity of the model and the complexity of the phenomena involved in the process.

### 6.3. *Test and simulation SHB-S*

In this test, displacements of the same magnitude were sequentially applied in the two orthogonal directions. Then, the specimen was unloaded to zero force in the same sequence. The imposed square-shaped loading path is shown in Fig. 13(a). In Fig. 13(b) is shown the experimental force $Z$–force $Y$ curve and in Fig. 13(c) the corresponding numerical simulation. The experimental force–displacement curves are indicated in Fig. 13(d) and (f) and the corresponding numerical simulations in Fig. 13(e) and (g).

### 6.4. *Test and simulation SHB-T*

In this test, displacements of the same magnitude were sequentially applied in the two orthogonal directions. Then, the specimen was unloaded simultaneously to zero force. The imposed triangular-shaped loading path is shown in Fig. 14(a). In Fig. 14(b) is shown the experimental force $Z$–force $Y$ curve and in Fig. 14(c) the corresponding numerical simulation. The experimental force–displacement curves are indicated in Fig. 14(d) and (f) and the corresponding numerical simulations in Fig. 14(e) and (g).

### 6.5. *Test and simulation SHB-C*

In this test, circular deflection paths were imposed as shown in Fig. 15(a). The experimental force $Z$–force $Y$ curve is indicated in Fig. 15(b). Fig. 15(c) shows the corresponding numerical simulation. The experimental force–displacement curves are indicated in Fig. 15(d) and (f) and the corresponding numerical simulations in Fig. 15(e) and (g).

## 7. Final remarks and conclusions

A model of the behavior of steel frame members with local buckling subjected to biaxial bending has been proposed. The model is extremely simple in spite of the complexity of the phenomena involved in the process. As a result, a quantitative measure of the degree of local buckling as well as a correct description of the mechanical behavior of the steel hollow structural elements is determined.

It can be noticed that only two additional constants (with respect to the conventional plasticity models) have been included in the model: $P_{cr}$ and $c$. These constants can be determined by using the procedure described in Section 5. This procedure is extremely simple and does not require the use of sophisticated equipment. The values of these constants could be measured for the most common commercial structural elements available in the market.

The model can be improved by the inclusion of the influence of the axial load in the local buckling evolution. This task is imperative if the model is going to be used for column analysis. As a first step, the local buckling parameters $P_{cr}$ and $c$ can be estimated as a function of the axial force. However the limitations of this simplified procedure remains to be proved experimentally. Probably, for moderate values of the axial forces a good enough precision for engineering purposes can be obtained.

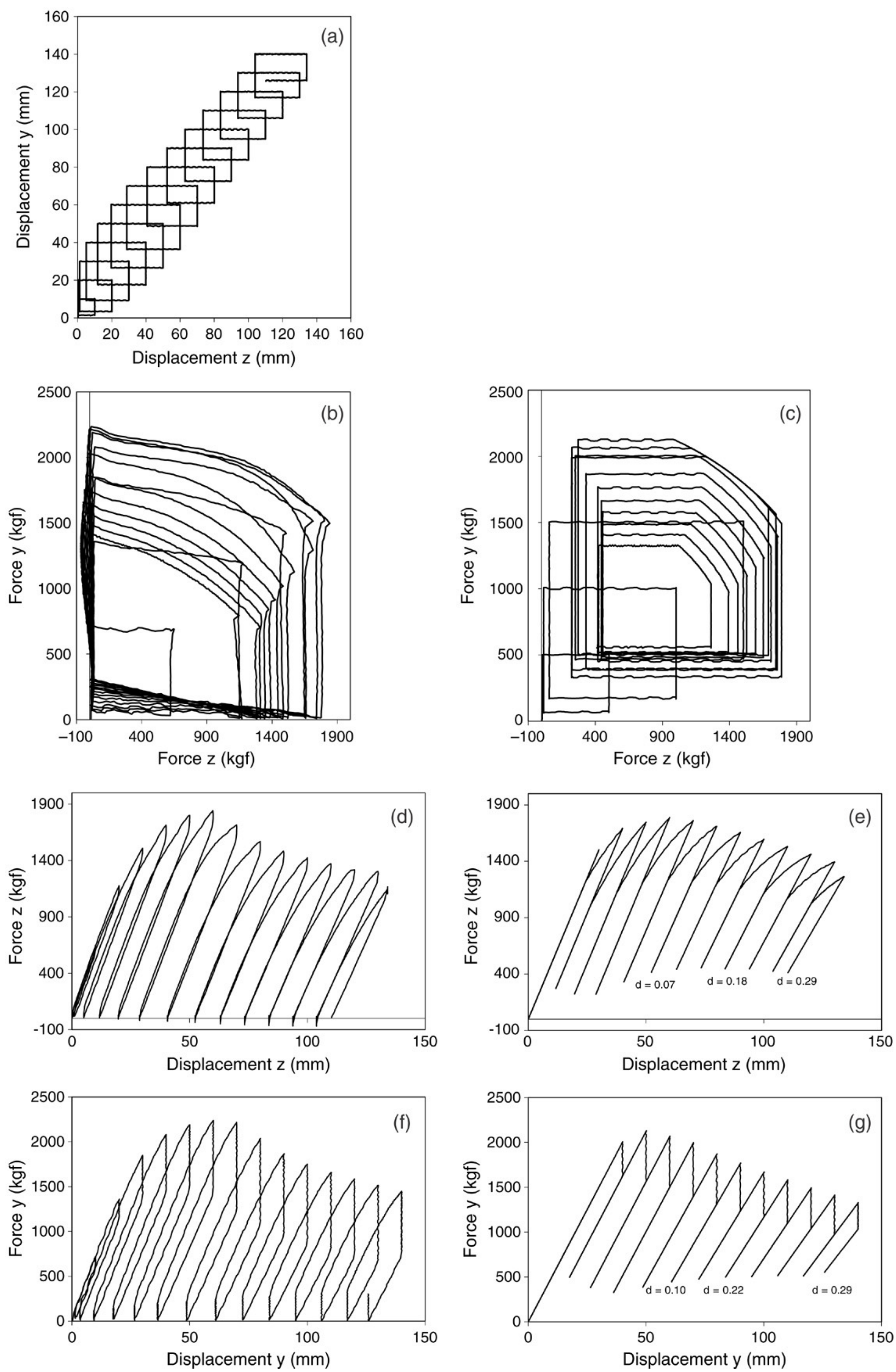


Fig. 13. Test and simulation SHB-S. (a) Imposed transverse displacements path. (b) Experimental force $Z$–force $Y$ curve. (c) Numerical simulation. (d) Experimental force–displacement curve in $Z$ direction. (e) Numerical simulation. (f) Experimental force–displacement curve in $Y$ direction. (g) Numerical simulation.

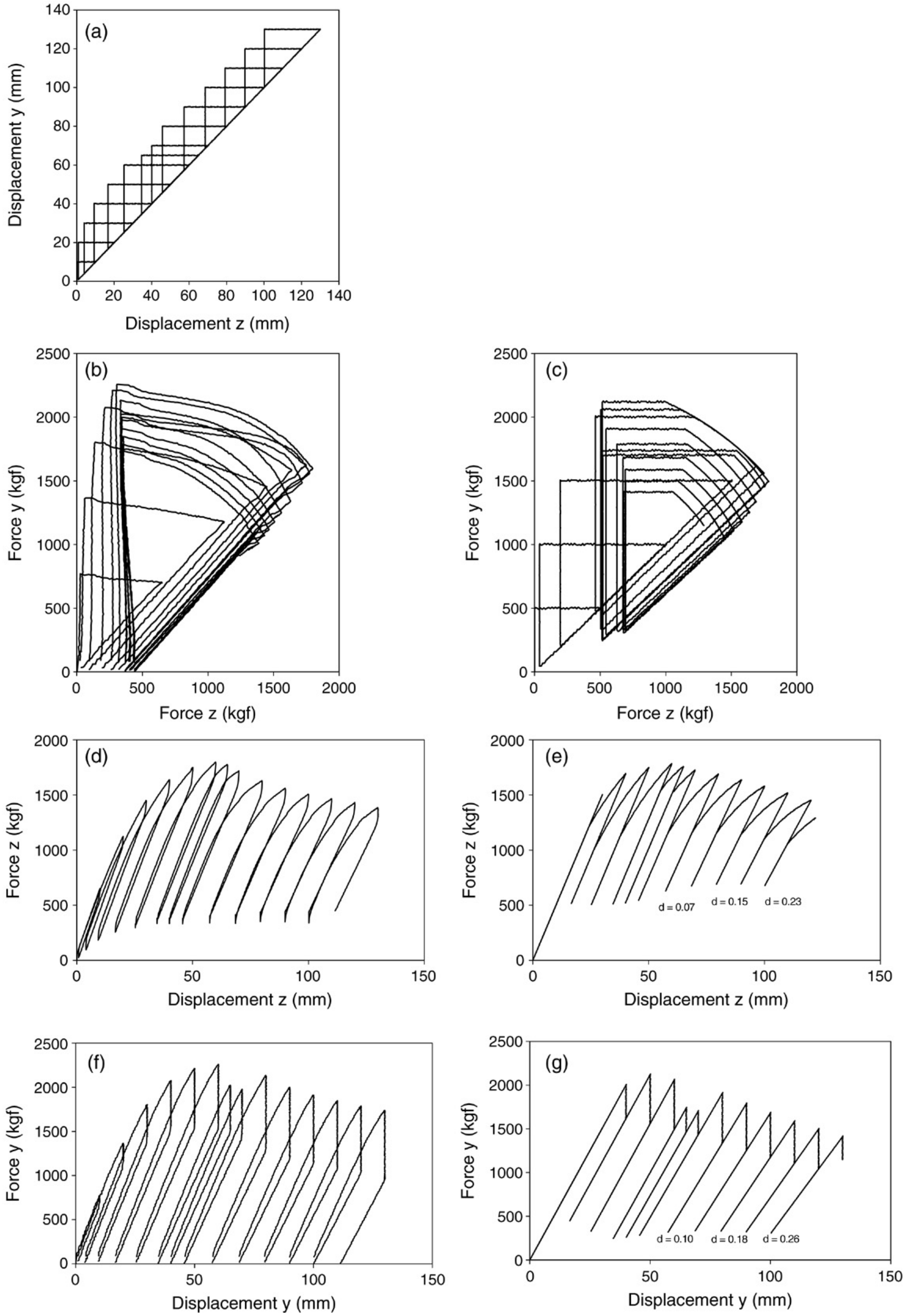


Fig. 14. Test and simulation SHB-T. (a) Imposed transverse displacements path. (b) Experimental force $Z$–force $Y$ curve. (c) Numerical simulation. (d) Experimental force–displacement curve in $Z$ direction. (e) Numerical simulation. (f) Experimental force–displacement curve in $Y$ direction. (g) Numerical simulation.

The plastic hardening process can also be included in the model. However this description would not influence the local buckling behavior of the elements except for non-compact members.

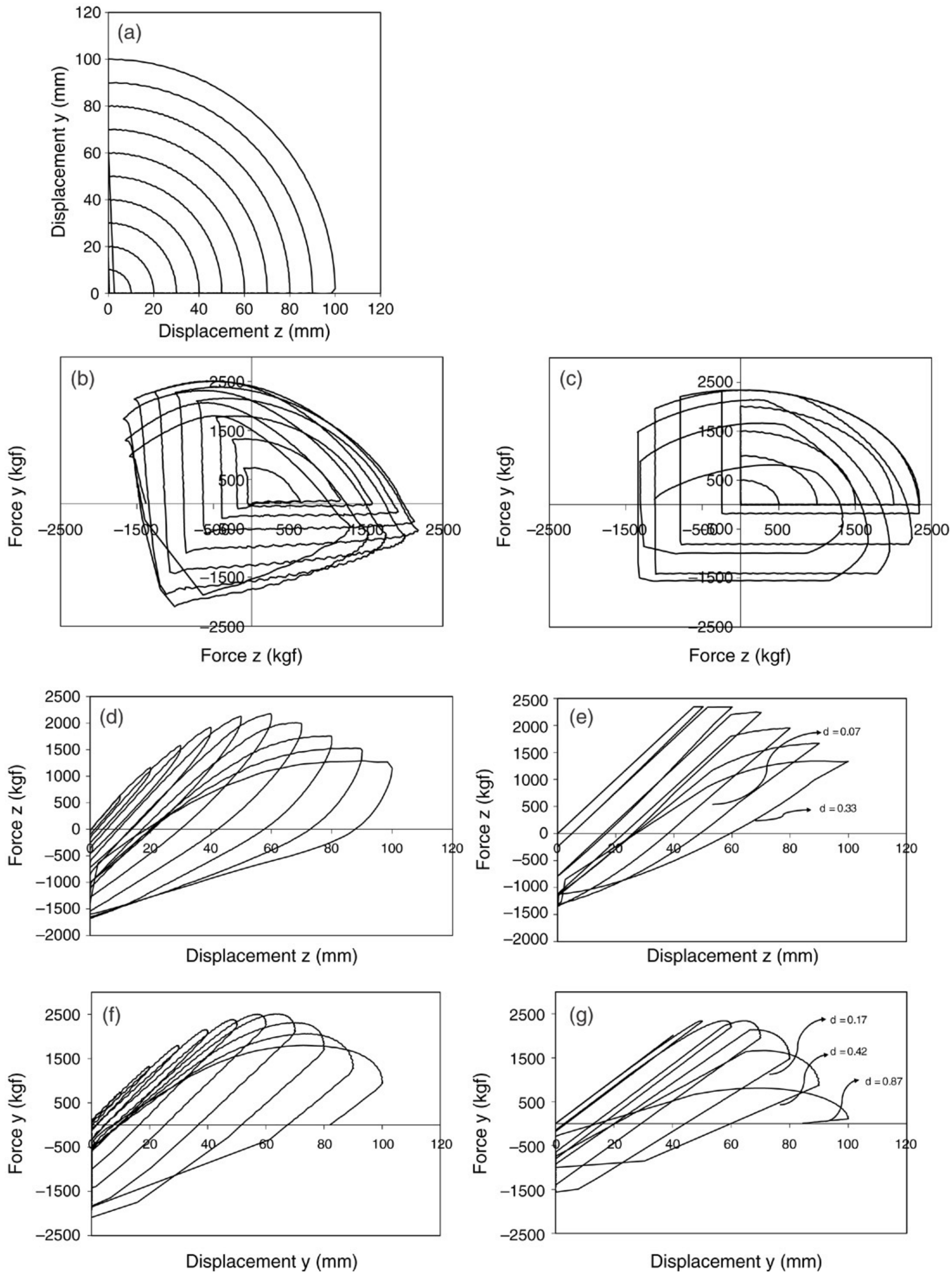


Fig. 15. Test and simulation SHB-C. (a) Imposed transverse displacement path. (b) Experimental force $Z$–force $Y$ curve. (c) Numerical simulation. (d) Experimental force–displacement curve in $Z$ direction. (e) Numerical simulation. (f) Experimental force–displacement curve in $Y$ direction. (g) Numerical simulation.

In structural elements with I-sections, there is significant torsion effects and torsion-induced buckling. These effects have not been considered in the model.

## Acknowledgements

The results presented in this paper were obtained in the course of an investigation sponsored by FONACIT and CDCHT-UCLA.

## References

[1] Davies JM. Strain hardening, local bucking and lateral–torsional bucking in plastic hinges. J Constr Steel Res 2006;62(1–2):27–34.

[2] Qin F, Fung TC, Soh CK. Hysteretic behavior of completely overlap tubular joints. J Constr Steel Res 2001;57(7):811–29.

[3] NISEE. Kobe geotechnical collection: Slide number KG47. National information service for earthquake engineering. Berkeley: University of California; 1998.

[4] Goggins JM, Broderick BM, Elghazouli AY, Lucas AS. Experimental cyclic response of cold-formed hollow steel bracing members. Eng Struct 2005;27(7):977–89.

[5] Okazaki T, Arce G, Ryu HC, Engelhardt MD. Experimental study of local bucking, overstrength, and fracture of links in eccentrically braced frames. J Struct Eng-ASCE 2005;131(10):1526–35.

[6] Nakashima M, Liu DW. Instability and complete failure of steel columns subjected to cyclic loading. J Eng Mech-ASCE 2005;131(6):559–67.

[7] Elchalakani M, Zhao XL, Grzebieta R. Test of cold-formed circular tubular braces under cyclic axial loading. J Struct Eng-ASCE 2003; 129(4):507–14.

[8] Broderick BM, Goggings JM, Elghazouli AY. Cyclic performance of steel and composite bracing members. J Constr Steel Res 2005;61(4):493–514.

[9] Goggings JM, Broderick BM, Elghazouli AY. Behaviour of tubular steel members under cyclic axial loading. J Struct Eng-ASCE 2006;62(1–2): 121–31.

[10] Lee CH, Jung JH, Oh MH, Koo ES. Experimental study of cyclic seismic behavior of steel moment connections reinforced with ribs. J Struct Eng-ASCE 2005;131(1):108–18.

[11] Lee SH, Choi NS. Bending performance evaluation of reinforced aluminum square tube beams considering local bucking behavior. In: Advances in fracture and strength, parts 1–4. Key engineering materials, vol. 297–300. 2005. p. 2290–6.

[12] Elchalakani M, Zhao XL, Grzebieta R. Cyclic bending tests to determine fully ductile section slenderness limits for cold-formed circular hollow sections. J Struct Eng-ASCE 2004;130(7):1001–10.

[13] Inglessis P, Gómez G, Quintero G, Flórez-López J. Model of damage for steel frame members. Eng Struct 1999;21(10):954–64.

[14] Febres R, Inglessis P, Flórez-López J. Modeling of local buckling in tubular steel frames subjected to cyclic loading. Comput Struct 2003;81: 2237–47.

[15] Inglessis P, Medina S, López A, Fébres R, Flórez-López J. Modeling of local buckling in tubular steel frames by using plastic hinges with damage. Steel Compos Struct 2002;2(1):21–34.

[16] Nakashima M, Matsumiya T, Suita K, Liu DW. Test on full-scale three-storey steel moment frame and assessment of ability of numerical simulation to trace cyclic inelastic behaviour. Earthquake Eng Struct D 2006;35(1):3–19.

[17] Kim SE, Kang KW. Large-scale testing of 3-D steel frame accounting for local buckling. Int J Solids Struct 2004;41(18–19):5003–22.

[18] Ju GT, Kyriakides S. Bifurcation and localization instabilities in cylindrical shells under bending — II Predictions. Int J Solids Struct 1992; 29(9):1143–71.

[19] Chan SL, Kitipornchai S, Faris GA. Elasto-plastic analysis of box-beam–columns including local buckling effects. J Struct Eng-ASCE 1991; 117(1):1946–62.

[20] Karamanos SA, Tassoulas JL. Tubular members. I: Stability analysis and preliminary results. J Eng Mech-ASCE 1996;122(1):64–71.

[21] Ellobody E, Young B. Structural performance of cold-formed high strength stainless steel columns. J Constr Steel Res 2005;61(12):1631–49.

[22] Salem AH, El Aghoury M, El Dib FF, Hanna MT. Ultimate capacity of I-slender section columns. J Constr Steel Res 2004;60(8):1193–211.

[23] Wilkinson T, Hancock G. Predicting the rotation capacity of cold-formed RHS beams using finite element analysis. J Constr Steel Res 2002;58(11): 1455–71.

[24] Sohal I, Chen WF. Moment–curvature expressions for fabricated tubes. J Struct Div- ASCE 1984;110(11):2738–57.

[25] Marante ME, Flórez-López J. Model of damage for RC elements subjected to biaxial bending. Eng Struct 2002;24(9):1141–52.

[26] Marante ME, Flórez-López J. Three-dimensional analysis of reinforced concrete frames based on lumped damage mechanics. Int J Solids Struct 2003;40(19):5119–23.

[27] Santathadaporn S, Chen WF. Interaction curves for section under combined biaxial bending and axial forces. Welding Research Council. Bulletin No. 148, New York; 1970.

[28] Guerrero N. Análisis de vigas de acero estructural de pared delgada sometidas a flexión biaxial. Doctoral thesis. Mérida (Venezuela): University of Los Andes [in preparation] [in Spanish].

[29] ABAQUS User's manual Hibbitt. Version 6.5-4. Karlsson & Sorensen, Inc.